

A Residual-Aware Theory of Position Bias in Transformers

Hanna Herasimchyk ^{*1} Robin Labryga ^{*1} Tomislav Prusina ^{*1} Sören Laue ¹

Abstract

Transformer models systematically favor certain token positions, yet the architectural origins of this position bias remain poorly understood. Under causal masking at infinite depth, prior theoretical analyses of attention rollout predict an inevitable collapse of attention onto the first token. Such collapse, however, does not occur in practice. We resolve this discrepancy with a residual-aware theory of cumulative attention rollout. By incorporating residual connections, we show that this architectural component prevents collapse under realistic conditions. At finite depth, we prove that causal Transformers induce a U-shaped position bias, with attention concentrating on early and late tokens. This provides a principled architectural explanation for the Lost-in-the-Middle phenomenon.

1. Introduction

Despite their widespread success, the mechanisms by which Transformers propagate information across depth remain poorly understood. In particular, modern Transformer models exhibit strong and systematic position biases that persist across tasks, inputs, and even lexical scrambling (Rahimi et al., 2026). These include a preference for early tokens (primacy bias), a preference for recent tokens (recency bias), and the widely observed Lost-in-the-Middle (LiM) phenomenon, in which information located in the center of long contexts is underutilized (Liu et al., 2024). A growing body of empirical evidence suggests that these effects are not primarily semantic, but instead reflect architectural structure.

Recent theoretical work has sought to explain position bias through attention rollout, interpreting stacked attention layers as a stochastic information propagation process across

^{*}Equal contribution ¹Department of Informatics, University of Hamburg, Hamburg, Germany. Correspondence to: Hanna Herasimchyk <hanna.herasimchyk@uni-hamburg.de>, Robin Labryga <robin.labryga@uni-hamburg.de>.

tokens. In a particularly influential analysis, Wu et al. (2025) show that, in attention-only causal Transformers, cumulative attention must collapse onto the first token as depth increases, independent of the choice of positional encodings. However, this prediction stands in direct contradiction to empirical observations in modern Transformer models, which do not exhibit such collapse even at substantial depth. This discrepancy between theory and practice is explicitly identified by Wu et al. (2025) as an open problem.

We argue that this gap arises from a fundamental modeling omission: existing theoretical analyses neglect residual connections, despite their central role in modern Transformer architectures. In this work, we develop a residual-aware theory of cumulative attention rollout that explicitly incorporates residual connections into cross-token information propagation. Within this framework, we identify and formally prove four architectural forces shaping position bias at finite depth: causal masking induces primacy effects; residual connections induce recency effects; relative positional biases such as ALiBi further favor recency; and coarse content contributions modulate these tendencies. Their interaction yields broad, often U-shaped influence profiles over input positions. Together, these architectural forces act as a structural prior that can give rise to the Lost-in-the-Middle phenomenon, even in the absence of semantic content. At infinite depth, the same framework shows that attention collapse is not inevitable, but depends on how attention mixing accumulates across layers.

Our analysis follows a coherent progression across increasingly realistic modeling assumptions. In the absence of residual connections, cumulative attention collapses onto the first token, as predicted by attention-only theory. Incorporating residual connections yields broad, typically U-shaped influence profiles. Adding a coarse content contribution, modeled as a constant plus diagonal self-attention systematically flattens these profiles. When we compare the predictions of this content-augmented, residual-aware theory to empirical estimates of input–output token influence in pre-trained language models, we find that the predicted profiles closely match the empirical ones. Together, these results bridge the gap between attention-only theory and practical Transformer behavior, providing an architecture-faithful framework for understanding position bias in modern sequence models.

Contributions.

- **Residual-aware attention rollout.** We introduce a residual-aware formulation of cumulative attention that explicitly models residual connections as persistent identity paths, yielding a propagation model aligned with modern Transformer architectures.
- **Architectural origin of position bias.** We show that Transformer architecture alone induces broad, often U-shaped influence profiles over input positions, establishing a structural prior consistent with empirically observed position-dependent effects even in the absence of content-dependent mechanisms.
- **Resolution of open problem (Wu et al. (ICML 2025))**
We show that the collapse of cumulative attention proven for attention-only causal Transformers (Wu et al., 2025) is not architecturally inevitable. Once residual connections are taken into account, collapse depends on the cumulative strength of attention mixing and may not occur.
- **Empirical validation against measured token influence.** We empirically validate our theoretical rollout model on pretrained language models by comparing its predicted influence profiles to empirically estimated input–output token influence. We find that the theory closely matches the observed distributions.

2. Related Work

Attention rollout and theoretical position bias. Attention rollout and information-flow perspectives have long been used to analyze Transformer behavior (Abnar & Zuidema, 2020; Chefer et al., 2021; Barbero et al., 2024). Most closely related to our work, Wu et al. (2025) provide a rigorous analysis of attention-only causal Transformers and prove that cumulative attention must collapse onto the first token as depth increases, independent of positional encoding choice. While elegant, this result is derived under an attention-only propagation model and does not incorporate residual connections. Empirically, such collapse is not observed in modern large-scale Transformers, motivating the need for a theory that closely reflects actual architectures.

Empirical primacy and recency bias. A substantial body of empirical work documents systematic position bias in Transformer attention, including primacy bias or “attention sinks” at early tokens (Zheng et al., 2023; Xiao et al., 2024; Yin et al., 2024; Guo et al., 2024; Kaul et al., 2025; Cobbina & Zhou, 2025) and recency bias favoring late tokens (Zhao et al., 2021; Sun et al., 2021; He et al., 2023; Liu et al., 2024). These effects are remarkably robust across inputs and tasks and persist even under lexical scrambling (Rahimi

et al., 2026), suggesting that they arise from architectural properties rather than semantic content. However, existing empirical studies do not provide a formal analysis of how such biases accumulate across depth in the presence of residual connections.

Positional encodings and bias modulation. Position bias has been studied empirically across a range of positional encoding schemes, including RoPE (Su et al., 2024) and ALiBi (Press et al., 2022; Kazemnejad et al., 2023). Empirical results show that the form and strength of position bias can vary substantially across layers and architectures (Yang et al., 2025), and that attention sinks can arise even in the absence of explicit positional encodings (Guo et al., 2024). These findings indicate that positional encodings modulate underlying architectural propagation effects, rather than fully determining position bias on their own.

Lost-in-the-Middle phenomena. The coexistence of primacy and recency biases gives rise to the Lost-in-the-Middle effect, where model performance degrades for information located in the center of long contexts (Liu et al., 2024; Guo & Vosoughi, 2025; Menschikov et al., 2025). Prior work characterizes this effect empirically and offers functional interpretations (Veseli et al., 2025; Salvatore et al., 2025), but does not provide a unified architectural explanation of how such U-shaped influence profiles arise.

Mitigating position bias. Several approaches aim to control position bias through architectural modifications or alternative attention mechanisms, such as reformulating softmax (Kaul et al., 2025) or introducing multi-scale positional encodings (Zhang et al., 2024). While effective in practice, these methods do not explain why such interventions are necessary from a structural standpoint. Our theory provides a principled perspective on the architectural origins of position bias that complements these approaches.

3. Notation and Problem Setup

We introduce notation and define a theory for analyzing how architectural components of Transformer models shape cumulative cross-token information propagation across layers, independent of training objectives, data, or optimization dynamics. Our framework is analytically tractable yet close to practical architectures. It explicitly models cross-token mixing, residual connections, attention masking, relative positional encodings, and coarse abstractions of content-dependent attention, while abstracting away token-wise components such as MLP blocks and layer normalization.

Tokens and layers. We consider a sequence of n tokens indexed by $i, j \in \{1, \dots, n\}$ and a Transformer of depth T , with attention layers indexed by $t \in \{1, \dots, T\}$.

Masks. Attention is constrained by a binary mask $\mathcal{M} \subseteq \{1, \dots, n\}^2$, where $(i, j) \in \mathcal{M}$ indicates that token i may attend to token j . We consider:

- **Causal masking:** $(i, j) \in \mathcal{M}$ iff $j \leq i$.
- **Sliding-window masking:** $(i, j) \in \mathcal{M}$ iff $i - w + 1 \leq j \leq i$ for a fixed window size w .

Attention matrices. At layer t , attention is represented by a row-stochastic matrix $A^{(t)} \in \mathbb{R}^{n \times n}$ with $A_{ij}^{(t)} = 0$ for $(i, j) \notin \mathcal{M}$. The entry $A_{ij}^{(t)}$ denotes the fraction of information token i draws from token j at layer t .

Throughout the theoretical analysis, we distinguish between per-input attention matrices and their dataset-averaged counterparts. If $A^{(t)}(x)$ denotes the attention matrix induced by an input x at layer t , we define the expected attention kernel

$$A^{(t)} := \mathbb{E}_x [A^{(t)}(x)].$$

All finite-depth results concern information propagation induced by these expected kernels.

Attention logits and content model. Attention weights are computed via a masked row-wise softmax

$$A_{i \cdot}^{(t)} = \text{softmax}(\ell_{i \cdot}^{(t)}),$$

with logits

$$\ell_{ij}^{(t)} = \begin{cases} s_{ij}^{(t)} + b_{ij}^{(t)}, & \text{if } (i, j) \in \mathcal{M}, \\ -\infty, & \text{otherwise.} \end{cases}$$

Here $b_{ij}^{(t)}$ captures position-dependent biases (e.g., relative positional encodings), while $s_{ij}^{(t)}$ captures content-dependent contributions. An explicit model for $s^{(t)}$ is specified later. We present single-head notation; the multi-head extension adds a head index (see Equation (4)).

Residual connections and mixing. Each attention layer in a Transformer is embedded in an additive residual block of the form

$$X^{(t+1)} = X^{(t)} + \text{Attn}(X^{(t)}),$$

which combines identity propagation with an attention-driven update. The attention operation aggregates information across tokens according to a row-stochastic attention matrix $A^{(t)}$; at the level of cross-token information propagation, attention thus induces a token-to-token mixing pattern governed by $A^{(t)}$, while feature-space transformations (e.g., value and output projections) act independently at each token and are abstracted away in the rollout analysis.

Residual handling in prior attention rollout work. Existing attention rollout formulations account for residual connections by explicitly augmenting the attention matrix with an identity contribution and renormalizing. In particular, Abnar and Zuidema (Abnar & Zuidema, 2020) replace $A^{(t)}$ by a fixed convex combination $\frac{1}{2}I + \frac{1}{2}A^{(t)}$ to account for residual connections.

Motivation for flexible residual mixing. From a dynamical-systems perspective, residual networks admit an interpretation as discretizations of continuous-time dynamics, commonly viewed through the lens of forward Euler schemes (Haber & Ruthotto, 2017; Chen et al., 2018). In numerical analysis, the choice of step size is not fixed a priori and is typically allowed to vary across steps to reflect the local magnitude of the update and ensure stable behavior (Hairer et al., 1993). This viewpoint motivates allowing the relative strength of the attention update to vary across layers and inputs, rather than fixing it heuristically.

Residual-aware transition with adaptive mixing. Since our analysis concerns only the relative contribution of the identity and attention paths, we normalize the additive update by total signal strength and define the residual mixing coefficient

$$\lambda_t(x) := \frac{\|\text{Attn}(X^{(t)})\|}{\|X^{(t)}\| + \|\text{Attn}(X^{(t)})\|}, \quad \lambda_t(x) \in [0, 1], \quad (1)$$

where $\|\cdot\|$ denotes the Frobenius norm. We use the Frobenius norm here, since it provides a stable measure of operator energy and is commonly used in analyses of residual networks and neural ODE discretizations to quantify typical propagation strength (Ruthotto & Haber, 2020).

In the theoretical analysis, we replace the input-dependent coefficient $\lambda_t(x)$ by its dataset expectation $\lambda_t := \mathbb{E}_x[\lambda_t(x)]$.

The resulting normalized update can be written as a convex combination of the identity stream and the attention stream, which induces the residual-aware transition matrix

$$R^{(t)} := (1 - \lambda_t)I + \lambda_t A^{(t)}. \quad (2)$$

By construction, $R^{(t)}$ is row-stochastic.

Importantly, because λ_t is defined in terms of the magnitude of the attention update, it implicitly captures the net effect of feature-space scaling operations within the attention block such as layer normalization and value/output projections on the relative strength of the attention path, without modeling these components explicitly.

Accordingly, the rollout operator defined below captures typical architectural information propagation under expected attention and residual mixing.

Cumulative rollout. Cumulative information propagation to layer T is captured by the rollout matrix

$$P^{(T)} := R^{(T)} R^{(T-1)} \dots R^{(1)}.$$

The entry $P_{ij}^{(T)}$ quantifies the total influence of input token j on token i after T layers. Under causal masking, the last-row distribution

$$p^{(T)}(j) := P_{nj}^{(T)} \quad (3)$$

measures the cumulative influence of input token j on the next output token.

This distribution is the central object studied in this paper: we analyze how architectural components, i.e., attention masking, positional encodings, and residual connections mathematically shape the rollout distribution $p^{(T)}$ at finite depth and determine whether it collapses in the infinite-depth limit.

4. Finite-Depth Attention Dynamics: Four Forces

To characterize systematic architectural effects at finite depth that shape the rollout distribution $p^{(T)}$, our analysis relies on the following weak positional monotonicity assumption on the dataset-averaged attention kernels, reflecting the ordering induced by causal masking while remaining agnostic to content and parameter values.

Assumption 4.1 (Stochastically monotone attention kernels). For each layer $t \in \{1, \dots, T\}$, let $A^{(t)} \in \mathbb{R}^{n \times n}$ denote the dataset-averaged attention kernel. We assume that $A^{(t)}$ is stochastically monotone (Definition A.1) with respect to the natural order on positions: for all $1 \leq i < i' \leq n$ and all prefix cutoffs $k \in \{1, \dots, n\}$,

$$\sum_{j=1}^k A_{ij}^{(t)} \geq \sum_{j=1}^k A_{i'j}^{(t)}.$$

Equivalently, for $i < i'$, the row distribution $A_{i,\cdot}^{(t)}$ is first-order stochastically smaller than $A_{i',\cdot}^{(t)}$.

This condition is naturally compatible with a broad class of attention mechanisms induced by causal masking and smoothly decaying or symmetric kernels. It is especially natural when $A^{(t)}$ is interpreted as an effective (head- and input-averaged) kernel that abstracts away content-dependent fluctuations and captures net architectural tendencies.

Although strict prefix-monotonicity is not always satisfied exactly, we empirically find that the effective kernels $A^{(t)}$ adhere to the condition up to numerically negligible deviations. Across models, layers, and datasets, violations are extremely rare, occurring for at most 10^{-6} of all triples

$(i < i', k)$. The mean conditional absolute prefix-mass gap is $\mathbb{E}[\Delta \mid \Delta > 0] \approx 2 \times 10^{-6}$, yielding an unconditional expected shortfall on the order of 10^{-12} . These results indicate that $A^{(t)}$ is extremely close to prefix-monotone in practice, supporting Assumption 4.1 as a stable regularity condition for the finite-depth force decomposition.

Under this regularity condition, the following propositions isolate the distinct architectural forces induced by masking, residual mixing, positional bias, and content structure.

Causal masking induces primacy drift. Causal masking introduces a directional asymmetry in information flow that, when composed across layers, systematically favors earlier positions in the rollout.

Proposition 4.2 (Primacy drift under causal and sliding-window masking). *Assume causal or causal sliding-window masking and Assumption 4.1. Let $p^{(t)}$ for $t \in \{1, \dots, T-1\}$ denote the last-row rollout distribution $p^{(t)}(j) = P_{nj}^{(t)}$. Then for every prefix length $k < n$, the prefix mass is monotonically increasing:*

$$\sum_{j=1}^k p^{(t+1)}(j) \geq \sum_{j=1}^k p^{(t)}(j).$$

Consequently, at finite depth the last-row rollout distribution exhibits a systematic drift of mass toward earlier positions.

Residual connections induce recency drift. Residual connections reduce cross-token mixing by preserving identity paths through depth. As a result, information is increasingly retained at its current position rather than propagated backward across the sequence, which biases finite-depth rollout toward recent tokens.

Proposition 4.3 (Residual strength induces recency drift). *Assume causal or causal sliding-window masking and Assumption 4.1. Fix attention kernels $\{A^{(t)}\}_{t=1}^T$ (interpreted as dataset-averaged operators) and consider two residual-mixing schedules $\{\lambda_t\}$ and $\{\lambda'_t\}$ with $\lambda_t \leq \lambda'_t$ for all t . Let $p^{(T)}$ and $p'^{(T)}$ denote the corresponding last-row rollout distributions. Then for every prefix length $k < n$,*

$$\sum_{j=1}^k p^{(T)}(j) \leq \sum_{j=1}^k p'^{(T)}(j).$$

Equivalently, strengthening residual connections (i.e., decreasing λ_t) induces a recency drift in the last-row rollout distribution.

Positional encodings induce recency drift. When positional encodings systematically prefer recent keys, they induce a recency bias that compounds across layers through rollout.

Proposition 4.4 (Positional encodings induce recency drift). *Assume causal (or sliding-window) masking. For each layer t , let*

$$A_0^{(t)} := \text{softmax}(s^{(t)}), \quad A_{\text{PE}}^{(t)} := \text{softmax}(s^{(t)} + b^{(t)}),$$

where positional logits $b_{ij}^{(t)}$ are recency-favoring in the sense that, for all admissible keys $j < k$,

$$b_{ij}^{(t)} \leq b_{ik}^{(t)}.$$

Assume Assumption 4.1 holds for $A_0^{(t)}$ (in the same dataset-averaged sense).

Let

$$R_0^{(t)} := (1 - \lambda_t)I + \lambda_t A_0^{(t)}, \quad R_{\text{PE}}^{(t)} := (1 - \lambda_t)I + \lambda_t A_{\text{PE}}^{(t)},$$

and denote the corresponding rollout distributions by $p_0^{(T)}$ and $p_{\text{PE}}^{(T)}$.

Then for every prefix length $k < n$,

$$\sum_{j=1}^k p_{\text{PE}}^{(T)}(j) \leq \sum_{j=1}^k p_0^{(T)}(j).$$

Equivalently, positional encodings induce a recency drift in the last-row rollout distribution.

Example (ALiBi). Under causal or sliding-window masking, ALiBi assigns larger biases to more recent keys for each query position. Consequently, ALiBi is recency-favoring and satisfies the assumptions of Proposition 4.4, implying a recency drift in the final rollout distribution.

Content contributions modulate positional drift. Content-dependent attention can induce highly task- and token-specific patterns that may either reinforce or counteract architectural biases. Without additional structure, no general monotonicity or drift guarantees are possible.

Instead, we adopt a restricted but empirically motivated abstraction in which content scores decompose into a constant background and a diagonal self-attention term at each layer. In Section 6, we empirically verify that this approximation provides a reasonable fit to measured content contributions in trained Transformer models.

Proposition 4.5 (Diagonal content induces a signed recency drift). *Assume causal (or sliding-window) masking. For each layer $t \in \{1, \dots, T\}$, suppose the content logits are*

$$s_{ij}^{(t)} = u^{(t)} + \delta^{(t)} \mathbb{1}_{\{j=i\}}, \quad (i, j) \in \mathcal{M},$$

with constants $u^{(t)}, \delta^{(t)} \in \mathbb{R}$. Let $A^{(t)}$ denote the dataset-averaged masked-softmax attention kernel induced by $\ell_{ij}^{(t)} =$

$b_{ij}^{(t)} + s_{ij}^{(t)}$, and let $R^{(t)} = (1 - \lambda_t)I + \lambda_t A^{(t)}$ with $\lambda_t \in [0, 1]$. Assume that the dataset-averaged baseline kernels $A^{(t)}|_{\delta^{(t)}=0}$ are stochastically monotone (hence so are $R^{(t)}|_{\delta^{(t)}=0}$).

Let $P^{(T)} = R^{(T)} \cdots R^{(1)}$. Then for any output position i and any $k < i$,

$$\forall t : \delta^{(t)} \geq 0 \Rightarrow \sum_{j=1}^k P_{ij}^{(T)} \leq \sum_{j=1}^k P_{ij}^{(T)}|_{\delta^{(1:T)} \equiv 0},$$

and

$$\forall t : \delta^{(t)} \leq 0 \Rightarrow \sum_{j=1}^k P_{ij}^{(T)} \geq \sum_{j=1}^k P_{ij}^{(T)}|_{\delta^{(1:T)} \equiv 0}.$$

Equivalently, positive diagonal content ($\delta^{(t)} > 0$) induces a recency drift, whereas negative diagonal content ($\delta^{(t)} < 0$) induces a primacy drift.

Structural forces and Lost-in-the-Middle. The above propositions identify architectural forces that shape attention at finite depth. When combined under causal rollout, these forces yield broad, non-collapsed influence profiles in which both early and recent tokens receive elevated influence relative to intermediate positions. This provides a purely structural explanation for Lost-in-the-Middle phenomena observed in the final layers of modern Transformer models, which we empirically confirm in Section 6.

5. Infinite-Depth Attention Dynamics

We now turn from finite- to infinite-depth attention dynamics. Wu et al. (2025) showed that under causal masking, attention collapses to the first token in the absence of residual mixing. Accounting for residual connections via a layer-dependent schedule yields a sharp dichotomy: collapse occurs if and only if the cumulative attention strength diverges. As in Wu et al. (2025), we adopt the same setting and assumptions, with no assumptions on positional encodings or content.

Assumption 5.1 (Bounded query and key operators). As in Wu et al. (2025), we assume there exists a constant $C > 0$ such that for all layers $t \geq 1$,

$$\|W_Q^{(t)}\|_2 \leq C, \quad \|W_K^{(t)}\|_2 \leq C,$$

where $\|\cdot\|_2$ is the operator norm.

Assumption 5.2 (Bounded value accumulation). As in Wu et al. (2025), we assume the sequence of value transformations is uniformly bounded in the sense that

$$\sup_{k \geq 1} \left\| \prod_{t=1}^k W_V^{(t)} \right\|_2 \leq C_V.$$

for some finite constant C_V .

Lemma 5.3 (Uniform Stability and Attention Lower Bound). *Suppose Assumptions 5.1-5.2 hold and the initial input is bounded such that $\|X^{(0)}\| \leq C$. Then there exist constants $C_X > 0$ and $\varepsilon > 0$, both independent of the depth t , such that for all $t \geq 1$:*

- (i) *The hidden states are uniformly bounded: $\max_i \|X_{i,:}^{(t)}\|_2 \leq C_X$.*
- (ii) *The attention weights are uniformly bounded away from zero: $A_{ij}^{(t)} \geq \varepsilon$ for all $(i, j) \in \mathcal{M}$.*

Theorem 5.4 (Residual-aware infinite-depth collapse dichotomy). *Under Assumptions 5.1-5.2, the asymptotic behavior of the residual-aware attention rollout $P^{(T)} := R^{(T)} \dots R^{(1)}$ is fully determined by the summability of the mixing coefficients $\{\lambda_t\}_{t \geq 1}$.*

- (i) **Finite total mixing implies no collapse.** If

$$\sum_{t=1}^{\infty} \lambda_t < \infty,$$

then for every token $i \in \{1, \dots, n\}$,

$$\liminf_{T \rightarrow \infty} P_{ii}^{(T)} \geq \prod_{t=1}^{\infty} (1 - (1 - \varepsilon) \lambda_t) > 0.$$

In particular, attention does not collapse to the first token, i.e., $\limsup_{T \rightarrow \infty} P_{i1}^{(T)} < 1$.

- (ii) **Infinite total mixing implies collapse.** If

$$\sum_{t=1}^{\infty} \lambda_t = \infty,$$

then for every token $i \in \{1, \dots, n\}$,

$$\lim_{T \rightarrow \infty} P_{i1}^{(T)} = 1.$$

Moreover, for all $1 < j \leq i$ and all $T \geq 1$, there exist constants $C' > 0$ and $\varepsilon > 0$, such that

$$P_{ij}^{(T)} \leq C' \exp\left(-(j-1)\varepsilon \sum_{s=1}^T \lambda_s\right),$$

and consequently $P_{ij}^{(T)} \rightarrow 0$ for all $j > 1$ as $T \rightarrow \infty$.

Discussion. Theorem 5.4 refines and strictly generalizes the infinite-depth collapse result of Wu et al. (2025), which is recovered as the special case $\lambda_t \equiv 1$ and hence $\sum_t \lambda_t = \infty$. The theorem shows that attention collapse under causal masking is not an intrinsic property of masked self-attention alone, but instead depends on the cumulative strength of layerwise attention mixing.

5.1. Multi-Head Extension

The finite-depth analysis in Section 4 and the infinite-depth analysis are formulated for a single attention head. In practice, Transformer layers employ multiple attention heads whose outputs are aggregated.

Let $A^{(t,h)}$ denote the causal row-stochastic attention kernel of head $h \in \{1, \dots, H\}$ at layer t , interpreted as the dataset-averaged kernel in the sense of Section 3. We model the effective attention operator at layer t as the uniform head average

$$A^{(t)} := \frac{1}{H} \sum_{h=1}^H A^{(t,h)}. \quad (4)$$

We use uniform weights for simplicity; more general convex combinations that account for head-specific output projections could also be justified, but are not needed for the theoretical results or the experiments presented here.

Since prefix masses, residual-aware transitions, and rollout operators depend linearly on the underlying attention kernel, all finite- and infinite-depth results established for a single head apply verbatim to $A^{(t)}$. In particular, convexity preserves causality, row-stochasticity, and the Assumption 4.1. For the infinite-depth analysis, we assume that Assumptions 5.1, and 5.2 hold uniformly across heads.

6. Empirical Validation

In this section, we empirically validate our finite-depth theory in three steps. First, we measure the model-dependent quantities required by the theory, namely the residual mixing schedule and the structure of content-dependent attention logits, confirming the assumptions and motivating the simplified content abstraction.

Second, we perform a controlled rollout computation to evaluate the predicted final-token influence distribution $p^{(T)}$ induced by our theory at realistic model depths. In this setting, we isolate architectural effects by applying the theoretical rollout using causal masking, residual connections, and positional encodings. We consider three controlled variants: (a) *attention-only rollout*, which omits residual connections and serves as a baseline; (b) *residual-aware rollout*, where content contributions to the attention logits are set to zero; and (c) *residual-aware rollout with constant content*, where content is incorporated using the empirically measured constant-plus-diagonal structure.

Third, we compare the resulting controlled rollout distributions to direct measurements of input token influence obtained from pre-trained models to empirically verify our theory.

Experimental setup. All experiments in this section are conducted on a common suite of pre-trained large language

Table 1. Architectural specifications of the causal, decoder-only Transformer models used in our experiments, including parameter count (in billions) and depth.

Model	Parameters (B)	Depth
falcon-rw-7b (Penedo et al., 2023)	7	36
mpt-7b (Mosaic, 2023a)	7	32
mpt-30b (Mosaic, 2023b)	30	48
bloom-7b (BigScience, 2022)	7	30
bloom-176b (BigScience, 2022)	176	70

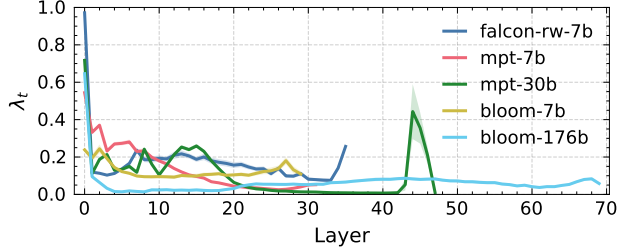


Figure 1. Depth-wise effective residual mixing coefficient λ_t in pre-trained LLMs. We report the mean \pm 95% confidence interval over 1,000 samples of length 2,048 from the FineWeb-Edu dataset. Most models exhibit decreasing attention contribution with depth.

models, including BLOOM, MPT, and Falcon, summarized in Table 1. We report averages over 1,000 prompts sampled from the FineWeb-Edu dataset (Penedo et al., 2024). Additional results using the DCLM-Baseline and Wikipedia datasets (Li et al., 2024; Foundation, 2026) are provided in the appendix.

Our code¹ is publicly available.

6.1. Measuring Residual Mixing and Content Structure in Pre-Trained LLMs

Effective residual mixing λ_t . We measure the residual mixing coefficient λ_t defined in Equation (1), which quantifies the relative contribution of attention-driven updates versus identity propagation at layer t . In the experiments, we report an empirical average of this quantity across inputs.

Concretely, we estimate

$$\lambda_t = \mathbb{E} \left[\frac{\|\text{Attn}(X^{(t)})\|}{\|X^{(t)}\| + \|\text{Attn}(X^{(t)})\|} \right], \quad (5)$$

where the expectation is taken over samples from the evaluation dataset. Figure 1 shows the estimates of λ_t across layers for selected pre-trained Transformer models. Additional results for different sequence lengths are provided in Appendix C.

Content logits structure for ALiBi models. We next examine the structure of the content-dependent attention logits

introduced in Section 3 and abstracted in our theoretical model (Proposition 4.5). We extract the content logits as the pre-softmax attention scores prior to the addition of the positional bias term and average them over prompts; corresponding heatmaps are shown in Appendix D. In addition, Table 6 in the appendix reports distributional similarity statistics that summarize these content logits across heads and layers. We find that, on average, the content logits are well approximated by a constant-plus-diagonal structure: off-diagonal entries are approximately uniform, while the diagonal exhibits a consistent global shift. This analysis is not intended to capture token-level or context-specific semantic effects, but rather to validate the coarse structural content abstraction used in our theory. In particular, it empirically supports modeling content contributions as a constant background term plus a diagonal self-attention component, as assumed in Proposition 4.5.

6.2. Controlled Rollout Computation

We compute the rollout matrix as defined in Section 3 and report the final-token influence distribution $p^{(T)}$ defined in Equation (3). All rollout computations match the architectural configuration of the corresponding pre-trained model, including depth, number of heads, masking pattern, and positional encoding. Heads are aggregated uniformly to form $A^{(t)}$ as in Equation (4). Where applicable, we use empirically measured layer-wise residual mixing schedules $\{\lambda_t\}$.

We consider three controlled variants of the same rollout experiment, illustrated in Figure 2, which progressively isolate the effects of residual connections and content.

Attention-only rollout. Residual connections are removed by setting $\lambda_t = 1$ for all layers and excluding content contributions. In this setting, the influence distribution collapses to the first token, reproducing the behavior predicted by prior attention-only analyses (Wu et al., 2025).

Residual-aware rollout. Residual connections are restored using the empirically measured schedules $\{\lambda_t\}$ while content contributions are still excluded. In this architecture-only setting, the rollout produces a broad U-shaped influence profile, demonstrating that residual connections prevent collapse and that causal masking, positional encodings, and residual mixing together induce a characteristic positional prior, even in the absence of content.

Residual-aware rollout with constant content. Content is incorporated using the empirically measured constant-plus-diagonal structure described in Section 6.1. Including content modulates the architectural prior by shifting mass toward later positions and reducing the primacy peak, while preserving the overall U-shaped profile.

¹<https://github.com/ml-uhh/position-bias>

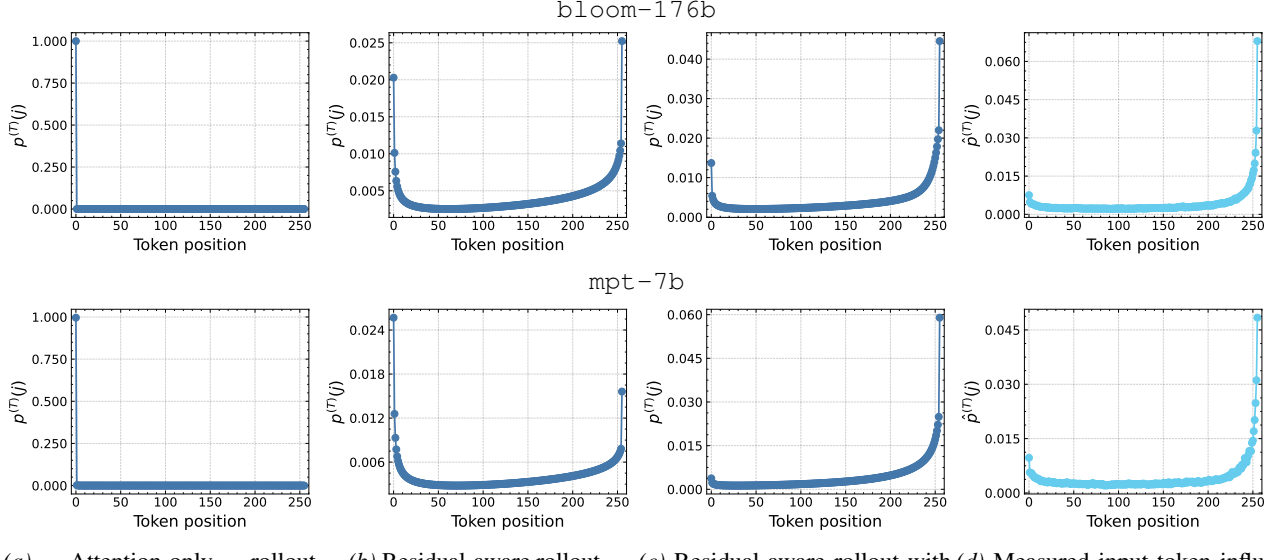


Figure 2. Final-token influence distributions $p^{(T)}$ for the 70-layer bloom-176b (top) and the 32-layer mpt-7b (bottom). Panels (a)–(c) show controlled rollout variants: (a) attention-only rollout ($\lambda_t = 1$, no content) exhibiting collapse to the first token; (b) residual-aware architectural rollout using measured schedules $\{\lambda_t\}$ (no content), producing a broad U-shaped profile; and (c) residual-aware rollout with empirically measured constant-plus-diagonal content, which modulates the U-shape by shifting mass toward later positions. Panel (d) shows the measured input token influence $\hat{p}^{(T)}$, which exhibits a similar U-shaped profile.

Taken together, these controlled rollouts isolate the distinct roles of attention-only dynamics, residual connections, and content. Residual connections are necessary to prevent collapse to the first token, architectural components alone induce a U-shaped positional prior, and content contributions modulate but do not eliminate this prior.

6.3. Measured Input Token Influence

We estimate input token influence using a gradient-based attribution method (Simonyan et al., 2014; Liu et al., 2026). For an input sequence x with embeddings e and predicted next token y , we define the influence of the j -th input token as

$$\hat{p}^{(T)}(j) = \mathbb{E}_x [\|\nabla_{e_j} P(y | x)\|_2], \quad (6)$$

and normalize across positions to obtain a probability distribution comparable to the controlled rollout. The expectation is taken over the samples from the evaluation dataset.

Figure 2d shows the measured input token influence for bloom-176b and mpt-7b. In both cases, the empirical distributions exhibit a U-shaped profile.

Qualitative validation. Consistent with the controlled analysis above, the residual-aware rollout without content (b) already reproduces the dominant U-shaped structure observed in the measured distribution (d). In particular, the location of the minimum of this curve often closely coincides with that of the empirical curve, confirming that the

Table 2. Spearman rank correlation (\uparrow higher is better) between predicted and gradient-based last-row influence distributions. Bold-face indicates the architectural variant closest to the measured influence distribution. (i.e., highest Spearman).

Model	(a) Attn. only	(b) Res.-aware	(c) Res.-aware + const. content
bloom-176b	-0.57	0.91	0.83
mpt-7b	-0.43	0.88	0.53

Table 3. Wasserstein distance (\downarrow lower is better) between predicted and gradient-based last-row influence distributions. Bold-face indicates the architectural variant closest to the measured influence distribution (i.e., lowest Wasserstein).

Model	(a) Attn. only	(b) Res.-aware	(c) Res.-aware + const. content
bloom-176b	0.65	0.08	0.01
mpt-7b	0.62	0.09	0.10

U-shaped positional prior arises from architectural mechanisms alone.

Incorporating the constant-plus-diagonal content abstraction (c) preserves this U-shape while slightly shifting mass toward more recent positions. Visually, this modulation leads to very close alignment between (c) and the measured distribution (d), particularly in larger models. By contrast, the attention-only rollout (a) collapses to the first token and fails to reproduce the empirical profile.

Quantitative validation. Tables 2 and 3 report Spearman rank correlation and Wasserstein distance between the rollout variants and the measured influence distribution, with additional per-dataset results provided in Appendix B (Tables 4 and 5).

Across models, the residual-aware rollout without content (b) often achieves the highest Spearman correlation, indicating that the architectural prior alone captures the dominant ordering of influential positions. The residual-aware rollout with constant content (c) typically attains comparable or lower Wasserstein distance, especially in larger models, reflecting improved geometric alignment of mass despite small local rank perturbations. As expected, the attention-only rollout (a) performs poorly under both metrics.

Together, these results indicate that Transformer architectures induce a U-shaped positional prior via residual connections, and that incorporating a coarse content abstraction further refines the geometric fit, bringing the theoretical rollout into close agreement with empirical measurements.

7. Discussion and Limitations

Architectural scope. Our analysis isolates architectural information propagation induced by attention, masking, positional encodings, and residual connections, abstracting away from training dynamics, optimization, and token semantics. The rollout framework focuses on token mixing structure rather than full representation dynamics. Accordingly, our results should be interpreted as characterizing architectural priors in Transformer models, not end-to-end representation learning.

Positional encodings. In the finite-depth analysis, we model attention logits as a sum of content-dependent terms and positional biases, capturing a broad class of additive positional encoding mechanisms. Empirically, we focus on ALiBi in controlled, content-free rollout experiments, as it instantiates this additive structure directly at the logit level. RoPE, in contrast, incorporates positional information through multiplicative transformations of queries and keys. While RoPE admits approximate disentanglements into positional and content-dependent factors, these approximations are generally too loose to yield comparably sharp finite-depth rollout characterizations. Developing tighter finite-depth probes for RoPE remains an open direction. Our infinite-depth results, however, do not rely on any assumptions about positional encodings and therefore apply equally to RoPE.

Lost-in-the-Middle. Our controlled rollouts show that U-shaped influence profiles can arise purely from architectural priors, providing a structural explanation for Lost-in-the-Middle behavior. At the same time, downstream task perfor-

mance depends on learned representations and objectives, which are not modeled in our analysis.

8. Conclusion

We developed a residual-aware theory of cumulative information propagation in Transformer models that characterizes positional bias at practical, finite depths. Our finite-depth analysis yields explicit, architecture-dependent characterizations that match the behavior observed in modern pre-trained language models. In controlled rollout experiments, the theory predicts broad, U-shaped influence profiles consistent with empirically observed Lost-in-the-Middle effects, demonstrating that such position bias can arise purely from architectural priors.

Beyond the finite-depth regime, we showed that incorporating residual connections fundamentally alters deep attention dynamics. In contrast to prior attention-only analyses that predict inevitable collapse, residual connections can prevent such collapse.

Impact Statement

This work advances the theoretical understanding of how architectural design choices in Transformer models shape information propagation across depth. By isolating the effects of causal masking, residual connections, positional biases, and simplified content contributions, the analysis clarifies the structural origins of well-documented position biases such as primacy, recency, and the Lost-in-the-Middle phenomenon. These insights can inform the principled design of future sequence models with more predictable and interpretable behavior, potentially improving robustness and performance on long-context tasks.

The results are primarily theoretical and diagnostic rather than prescriptive. They do not introduce new training procedures or model architectures, but instead provide tools for reasoning about existing ones. As such, the work does not present direct risks related to misuse, deployment, or societal harm beyond those already associated with large-scale Transformer models. By improving transparency around architectural biases, this work may contribute to better debugging and evaluation practices, which can indirectly support safer and more reliable model development.

No immediate negative societal impacts are anticipated.

References

- Abnar, S. and Zuidema, W. Quantifying attention flow in transformers. In *ACL*, 2020.
- Barbero, F., Banino, A., Kapiturowski, S., Kumaran, D., Madeira Araújo, J., Vitvitskyi, O., Pascanu, R., and

Veličković, P. Transformers need glasses! information over-squashing in language tasks. In *NeurIPS*, 2024.

BigScience, L. Bigscience language open-science open-access multilingual (bloom) language model, 2022.

Chefer, H., Gur, S., and Wolf, L. Transformer interpretability beyond attention visualization. In *CVPR*, 2021.

Chen, R. T. Q., Rubanova, Y., Bettencourt, J., and Duvenaud, D. Neural ordinary differential equations. In *NeurIPS*, 2018.

Cobbina, K. A. and Zhou, T. Where to show demos in your prompt: A positional bias of in-context learning. In *EMNLP*, 2025.

Foundation, W. Wikimedia downloads, January 2026. URL <https://dumps.wikimedia.org>.

Guo, T., Pai, D., Bai, Y., Jiao, J., Jordan, M. I., and Mei, S. Active-dormant attention heads: Mechanistically demystifying extreme-token phenomena in llms. In *arXiv preprint arXiv:2410.13835*, 2024.

Guo, X. and Vosoughi, S. Serial position effects of large language models. In *ACL*, 2025.

Haber, E. and Ruthotto, L. Stable architectures for deep neural networks. *Inverse Problems*, 34(1):014004, 2017.

Hairer, E., Nørsett, S. P., and Wanner, G. *Solving Ordinary Differential Equations I: Nonstiff Problems*. Springer, 2 edition, 1993.

He, B., Martens, J., Zhang, G., Botev, A., Brock, A., Smith, S., and Teh, Y. Deep transformers without shortcuts: Modifying self-attention for faithful signal propagation. In *ICLR*, 2023.

Kaul, P., Ma, C., Elezi, I., and Deng, J. From attention to activation: Unravelling the enigmas of large language models. In *ICLR*, 2025.

Kazemnejad, A., Padhi, I., Natesan Ramamurthy, K., Das, P., and Reddy, S. The impact of positional encoding on length generalization in transformers. In *NeurIPS*, 2023.

Li, J., Fang, A., Smyrnis, G., Ivgi, M., Jordan, M., Gadre, S., Bansal, H., Guha, E., Keh, S., Arora, K., Garg, S., Xin, R., Muennighoff, N., Heckel, R., Mercat, J., Chen, M., Gururangan, S., Wortsman, M., Albalak, A., Bitton, Y., Nezhurina, M., Abbas, A., Hsieh, C.-Y., Ghosh, D., Gardner, J., Kilian, M., Zhang, H., Shao, R., Pratt, S., Sanyal, S., Ilharco, G., Daras, G., Marathe, K., Gokaslan, A., Zhang, J., Chandu, K., Nguyen, T., Vasiljevic, I., Kakade, S., Song, S., Sanghavi, S., Faghri, F., Oh, S., Zettlemoyer, L., Lo, K., El-Nouby, A., Pouransari, H., Toshev, A., Wang, S., Groeneveld, D., Soldaini, L., Koh, P. W., Jitsev, J., Kollar, T., Dimakis, A. G., Carmon, Y., Dave, A., Schmidt, L., and Shankar, V. Datacomp-lm: In search of the next generation of training sets for language models. In *NeurIPS*, 2024.

Liu, N. F., Lin, K., Hewitt, J., Paranjape, A., Bevilacqua, M., Petroni, F., and Liang, P. Lost in the middle: How language models use long contexts. In *Transactions of the Association for Computational Linguistics*, volume 12, pp. 157–173, 2024.

Liu, T. J. B., Zadeoğlu, B., Bouillé, N., Sarfati, R., and Earls, C. J. Jacobian scopes: token-level causal attributions in llms. In *arXiv preprint arXiv:2601.16407*, 2026.

Menschikov, M., Kharitonov, A., Kotyga, M., Porvatov, V., Zhukovskaya, A., Kagramanyan, D., Shvetsov, E., and Burnaev, E. Beyond early-token bias: Model-specific and language-specific position effects in multilingual llms. In *arXiv preprint arXiv:2505.16134*, 2025.

Mosaic. Introducing MPT-7b: A new standard for open-source, commercially usable LLMs, May 2023a. URL <https://www.databricks.com/blog/mpt-7b>. Databricks Blog.

Mosaic. MPT-30b: Raising the bar for open-source foundation models, June 2023b. URL <https://www.databricks.com/blog/mpt-30b>. Databricks Blog.

Penedo, G., Malartic, Q., Hesslow, D., Cojocaru, R., Capelli, A., Alobeidli, H., Pannier, B., Almazrouei, E., and Launay, J. The RefinedWeb dataset for Falcon LLM: outperforming curated corpora with web data, and web data only. In *arXiv preprint arXiv:2306.01116*, 2023.

Penedo, G., Kydlíček, H., Lozhkov, A., Mitchell, M., Raffel, C. A., Von Werra, L., Wolf, T., et al. The fineweb datasets: Decanting the web for the finest text data at scale. In *NeurIPS*, 2024.

Press, O., Smith, N. A., and Lewis, M. Train short, test long: Attention with linear biases enables input length extrapolation. In *ICLR*, 2022.

Rahimi, M., Nouri, M., and Yaghoobzadeh, Y. Layer-wise positional bias in short-context language modeling. In *arXiv preprint arXiv:2601.04098*, 2026.

Ruthotto, L. and Haber, E. Deep neural networks motivated by partial differential equations. *J. Math. Imaging Vis.*, 62(3):352–364, 2020.

Salvatore, N., Wang, H., and Zhang, Q. Lost in the middle: An emergent property from information retrieval demands in llms. In *arXiv preprint arXiv:2510.10276*, 2025.

Simonyan, K., Vedaldi, A., and Zisserman, A. Deep inside convolutional networks: Visualising image classification models and saliency maps. In *ICLR*, 2014.

Su, J., Ahmed, M., Lu, Y., Pan, S., Bo, W., and Liu, Y. Roformer: Enhanced transformer with rotary position embedding. *Neurocomputing*, 568:127063, 2024.

Sun, S., Krishna, K., Mattarella-Micke, A., and Iyyer, M. Do long-range language models actually use long-range context? In *EMNLP*, 2021.

Veseli, B., Chibane, J., Toneva, M., and Koller, A. Positional biases shift as inputs approach context window limits. In *COLM*, 2025.

Wu, X., Wang, Y., Jegelka, S., and Jadbabaie, A. On the emergence of position bias in transformers. In *ICML*, 2025.

Xiao, G., Tian, Y., Chen, B., Han, S., and Lewis, M. Efficient streaming language models with attention sinks. In *ICLR*, 2024.

Yang, B., Venkitesh, B., Talupuru, D., Lin, H., Cairuz, D., Blunsom, P., and Locatelli, A. Rope to nope and back again: A new hybrid attention strategy. In *NeurIPS*, 2025.

Yin, Q., He, X., Zhuang, X., Zhao, Y., Yao, J., Shen, X., and Zhang, Q. Stablemask: Refining causal masking in decoder-only transformer. In *ICML*, 2024.

Zhang, Z., Chen, R., Liu, S., Yao, Z., Ruwase, O., Chen, B., Wu, X., Wang, Z., et al. Found in the middle: How language models use long contexts better via plug-and-play positional encoding. In *NeurIPS*, 2024.

Zhao, Z., Wallace, E., Feng, S., Klein, D., and Singh, S. Calibrate before use: Improving few-shot performance of language models. In *ICML*, 2021.

Zheng, L., Chiang, W.-L., Sheng, Y., Zhuang, S., Wu, Z., Zhuang, Y., Lin, Z., Li, Z., Li, D., Xing, E. P., Zhang, H., Gonzalez, J. E., and Stoica, I. Judging llm-as-a-judge with mt-bench and chatbot arena. In *NeurIPS*, 2023.

Appendix Overview

The appendix is organized as follows.

Appendix A contains the complete proofs of all theoretical results.

Appendix B provides additional results on cumulative rollout distributions and its quantitative analysis.

Appendix C offers further results on residual mixing schedules.

Appendix D presents qualitative content heatmaps and corresponding similarity statistics.

A. Proofs of Theoretical Results

This appendix contains the proofs of the finite-depth propositions from Section 4 and the infinite-depth theorem stated in Section 5.

A.1. Proofs of Section 4 (Finite-Depth Case)

First, we need to state a few definitions and lemmas that we will use in the proofs.

Stochastic order on positions. Let μ, ν be probability distributions on $\{1, \dots, n\}$. We write

$$\mu \succeq_{\text{FOSD}} \nu \quad (\text{first-order stochastic dominance}) \iff \sum_{j=1}^m \mu(j) \leq \sum_{j=1}^m \nu(j) \quad \forall m \in \{1, \dots, n\}.$$

Thus $\mu \succeq_{\text{FOSD}} \nu$ means that μ is shifted toward *larger indices* (more recent tokens). Equivalently, for every monotonically increasing test function $\varphi : \{1, \dots, n\} \rightarrow \mathbb{R}$,

$$\mu \succeq_{\text{FOSD}} \nu \iff \mathbb{E}_{X \sim \mu}[\varphi(X)] \geq \mathbb{E}_{X \sim \nu}[\varphi(X)]. \quad (7)$$

(Here $\mathbb{E}_{X \sim \mu}[\varphi(X)] = \sum_{j=1}^n \mu(j)\varphi(j)$, and similarly for ν .)

Kernels and rollout. A row-stochastic matrix $K \in \mathbb{R}^{n \times n}$ is viewed as a Markov kernel on $\{1, \dots, n\}$. For a distribution μ (row vector), μK denotes the pushforward distribution. In our setting, the layer operator is

$$R^{(t)} = (1 - \lambda_t)I + \lambda_t A^{(t)},$$

where $A^{(t)}$ is row-stochastic (attention) and $\lambda_t \in [0, 1]$. The rollout distribution of the final token after T layers is

$$\mu_T^\top = e_n^\top P^{(T)} = e_n^\top R^{(T)} R^{(T-1)} \dots R^{(1)}.$$

Throughout Appendix A.1, the attention kernels $A^{(t)}$ are understood in the same sense as in Section 3 and Section 4: namely, $A^{(t)} := \mathbb{E}_x[A^{(t)}(x)]$ denotes the dataset-averaged (expected) attention kernel. All arguments below are deterministic and apply to these expected kernels.

Definition A.1 (Stochastically monotone (isotone) kernel). A row-stochastic kernel K is *stochastically monotone* if its row laws are monotone in FOSD:

$$i < i' \implies K(i, \cdot) \preceq_{\text{FOSD}} K(i', \cdot).$$

Equivalently, for every monotonically increasing φ , the function $g_\varphi(i) := \sum_{j=1}^n K(i, j)\varphi(j)$ is monotonically increasing in i .

Lemma A.2 (Order preservation under a stochastically monotone kernel). *Let K be stochastically monotone. If $\mu \succeq_{\text{FOSD}} \nu$, then*

$$\mu K \succeq_{\text{FOSD}} \nu K.$$

Proof. Fix any monotonically increasing φ . Let $g(i) := \sum_j K(i, j)\varphi(j)$. By Definition A.1, g is monotonically increasing. Using Equation (7),

$$\mathbb{E}_{X \sim \mu K}[\varphi(X)] = \sum_i \mu(i)g(i) \geq \sum_i \nu(i)g(i) = \mathbb{E}_{X \sim \nu K}[\varphi(X)].$$

Since this holds for all monotonically increasing φ , $\mu K \succeq_{\text{FOSD}} \nu K$ by Equation (7). \square

Lemma A.3 (Residual kernels inherit stochastic monotonicity). *If A is stochastically monotone, then for any $\lambda \in [0, 1]$ the residual kernel $R_\lambda = (1 - \lambda)I + \lambda A$ is also stochastically monotone.*

Proof. Fix a monotonically increasing φ and define $g_A(i) := \sum_j A(i, j)\varphi(j)$. Since A is stochastically monotone, g_A is monotonically increasing. For R_λ ,

$$g_{R_\lambda}(i) := \sum_j R_\lambda(i, j)\varphi(j) = (1 - \lambda)\varphi(i) + \lambda g_A(i),$$

which is monotonically increasing as a convex combination of monotonically increasing functions. Hence R_λ is stochastically monotone. \square

Lemma A.4 (Rowwise dominance implies dominance after one step). *Let K, K' be row-stochastic kernels. Assume row-wise dominance, i.e., for all i ,*

$$K(i, \cdot) \succeq_{\text{FOSD}} K'(i, \cdot).$$

Then for any distribution μ ,

$$\mu K \succeq_{\text{FOSD}} \mu K'.$$

Proof. Fix a monotonically increasing φ and define $g(i) := \sum_j K(i, j)\varphi(j)$ and $g'(i) := \sum_j K'(i, j)\varphi(j)$. By the row-wise dominance assumption and Equation (7), $g(i) \geq g'(i)$ for all i . Therefore,

$$\mathbb{E}_{X \sim \mu K}[\varphi(X)] = \sum_i \mu(i)g(i) \geq \sum_i \mu(i)g'(i) = \mathbb{E}_{X \sim \mu K'}[\varphi(X)].$$

\square

Lemma A.5 (Monotone-vector propagation). *If K is stochastically monotone and $v \in \mathbb{R}^n$ is monotonically decreasing in its index, then Kv is monotonically decreasing.*

Proof. For $i < i'$, $K(i, \cdot) \preceq_{\text{FOSD}} K(i', \cdot)$. Taking $\varphi = -v$ (which is monotonically increasing since v is monotonically decreasing) and using Equation (7) yields $\sum_j K(i, j)(-v_j) \leq \sum_j K(i', j)(-v_j)$, i.e. $(Kv)_i \geq (Kv)_{i'}$. \square

A.1.1. PRIMACY DRIFT UNDER CAUSAL / SLIDING-WINDOW MASKING

Proof of Proposition 4.2. Fix $k < n$ and define $\mathbf{1}_k \in \mathbb{R}^n$ by $(\mathbf{1}_k)_j = \mathbb{1}_{\{j \leq k\}}$. Let $m^{(t)} := P^{(t)}\mathbf{1}_k$, so that the final-token prefix mass equals

$$\sum_{j \leq k} \mu_t(j) = e_n^\top P^{(t)} \mathbf{1}_k = m_n^{(t)}.$$

Since each $A^{(t)}$ is stochastically monotone by Assumption 4.1 (in expectation), Lemma A.3 implies each $R^{(t)}$ is also stochastically monotone.

Since $\mathbf{1}_k$ is monotonically decreasing and $m^{(t+1)} = R^{(t+1)}m^{(t)}$, Lemma A.5 implies $m^{(t)}$ is monotonically decreasing for every t . Hence, $m_i^{(t)} \geq m_n^{(t)}$ for all i . Using row-stochasticity,

$$m_n^{(t+1)} = \sum_{i=1}^n R_{ni}^{(t+1)} m_i^{(t)} \geq \sum_{i=1}^n R_{ni}^{(t+1)} m_n^{(t)} = m_n^{(t)},$$

which proves that the final-token prefix mass $\sum_{j \leq k} \mu_t(j)$ is monotonically increasing in depth. \square

A.1.2. STRONGER RESIDUAL (SMALLER λ) INDUCES RECENTY DRIFT

Proof of Proposition 4.3. Fix a layer and write $R_\lambda = (1 - \lambda)I + \lambda A$, where A is row-stochastic and causal (or sliding-window), so that $\text{supp}(A(i, \cdot)) \subseteq \{1, \dots, i\}$ for each i . Under our convention that larger indices are more recent, for any distribution ν supported on $\{1, \dots, i\}$ we have $\delta_i \succeq_{\text{FOSD}} \nu$, where δ_i is the Kronecker delta. Therefore, for any $0 \leq \lambda \leq \lambda' \leq 1$ and each i ,

$$R_\lambda(i, \cdot) = (1 - \lambda)\delta_i + \lambda A(i, \cdot) \succeq_{\text{FOSD}} (1 - \lambda')\delta_i + \lambda' A(i, \cdot) = R_{\lambda'}(i, \cdot). \quad (8)$$

Now compare two schedules $\{\lambda_t\}$ and $\{\lambda'_t\}$ with $\lambda_t \leq \lambda'_t$ for all t . Let μ_t and μ'_t be the corresponding rollout distributions of the final token. Applying Lemma A.4 at each step with $K = R_{\lambda_t}^{(t)}$ and $K' = R_{\lambda'_t}^{(t)}$ and using Equation (8) yields $\mu_t \succeq_{\text{FOSD}} \mu'_t$ inductively. In particular, $\mu_T \succeq_{\text{FOSD}} \mu'_T$, i.e., stronger residual (smaller λ) produces a more recent rollout law. \square

A.1.3. RECENTY-FAVORING POSITIONAL ENCODINGS INDUCE RECENTY DRIFT

Proof of Proposition 4.4. Fix a layer t and an input x drawn from the data distribution. Let $A_0^{(t)}(x)$ and $A_{\text{PE}}^{(t)}(x)$ denote the per-input attention kernels without and with positional encoding, respectively. We first establish the claimed rowwise dominance for each fixed x , and then take expectations over x .

Fix i and a support interval J_i . Let π_θ be the softmax row distribution on J_i given by

$$\pi_\theta(j) \propto \exp(s_{ij}(x) + \theta b_{ij}), \quad j \in J_i,$$

where b_{ij} is *monotonically increasing in j* (recency-favoring). For $m \in \{1, \dots, n\}$ define the prefix indicator $h_m(j) = \mathbb{1}_{\{j \leq m\}}$, and observe that $\mathbb{E}_{\pi_\theta}[h_m(j)]$ denotes the prefix mass under π_θ .

A standard softmax derivative identity gives

$$\frac{\partial}{\partial \theta} \mathbb{E}_{\pi_\theta}[h_m(j)] = \text{Cov}_{\pi_\theta}(h_m(j), b_{ij}).$$

Let $H = \{j \leq m\}$. Since b_{ij} is monotonically increasing in j , we have $\mathbb{E}[b_{ij} \mid H] \leq \mathbb{E}[b_{ij} \mid H^c]$, hence $\mathbb{E}[b_{ij}] \geq \mathbb{E}[b_{ij} \mid H]$ and therefore

$$\text{Cov}_{\pi_\theta}(1_H, b_{ij}) = \mathbb{P}(H)(\mathbb{E}[b_{ij} \mid H] - \mathbb{E}[b_{ij}]) \leq 0.$$

Therefore, the prefix mass $\mathbb{E}_{\pi_\theta}[h_m(j)]$ is monotonically decreasing in θ , and thus for $\theta_2 \geq \theta_1$,

$$\pi_{\theta_2} \succeq_{\text{FOSD}} \pi_{\theta_1}.$$

Consequently, for each fixed input x , the attention kernel rows satisfy

$$A_{\text{PE}}^{(t)}(x)(i, \cdot) \succeq_{\text{FOSD}} A_0^{(t)}(x)(i, \cdot) \quad \text{for all } i.$$

Taking expectations over x preserves these prefix inequalities, and hence the dataset-averaged kernels satisfy

$$A_{\text{PE}}^{(t)}(i, \cdot) \succeq_{\text{FOSD}} A_0^{(t)}(i, \cdot) \quad \text{for all } i.$$

Now fix depth T and compare a model with PE to the baseline without PE. For each layer t , the corresponding residual kernels satisfy the same rowwise dominance, $R_{\text{PE}}^{(t)}(i, \cdot) \succeq_{\text{FOSD}} R_0^{(t)}(i, \cdot)$ for all i . Applying Lemma A.4 at layer $t = 1$ yields $\mu_1^{(\text{PE})} \succeq_{\text{FOSD}} \mu_1^{(0)}$. Inductively repeating this argument across layers gives $\mu_T^{(\text{PE})} \succeq_{\text{FOSD}} \mu_T^{(0)}$, which proves that recency-favoring positional encodings induce a recency drift in the rollout distribution. \square

A.1.4. CONTENT CONTRIBUTIONS MODULATE POSITIONAL DRIFT

Proof of Proposition 4.5. We write A_δ for the (dataset-averaged) attention matrix in a given layer when the content contribution is of the form ‘‘constant plus diagonal’’, i.e.,

$$\ell_{ij} = s_{ij} + b_{ij} = c + \delta \mathbb{1}_{\{j=i\}} + b_{ij}, \quad A_\delta(i, \cdot) = \text{softmax}(\ell_{i \cdot}),$$

and define the corresponding residual kernel $R_\delta := (1 - \lambda)I + \lambda A_\delta$. Let A_0, R_0 denote the baseline ($\delta = 0$) matrices. Fix a row i and a cutoff $m < i$. Consider the prefix mass

$$\sum_{j \leq m} A_\delta(i, j).$$

Since the additive constant c cancels in the softmax normalization, we may drop it. Writing

$$Z_i(\delta) := \sum_{j \in \mathcal{J}_i} \exp(\delta \mathbb{1}_{\{j=i\}} + b_{ij}) = \exp(\delta + b_{ii}) + \sum_{j \in \mathcal{J}_i \setminus \{i\}} \exp(b_{ij}),$$

where $\mathcal{J}_i \subseteq \{1, \dots, i\}$ is the set of admissible keys under the (masked) attention pattern, we obtain for any $m < i$ (so $i \not\leq m$):

$$F_i(m; \delta) = \frac{\sum_{j \in \mathcal{J}_i, j \leq m} \exp(b_{ij})}{Z_i(\delta)}.$$

The numerator is independent of δ , hence

$$\frac{\partial}{\partial \delta} \sum_{j \leq m} A_\delta(i, j) = -\frac{\sum_{j \in \mathcal{J}_i, j \leq m} \exp(b_{ij})}{Z_i(\delta)^2} \exp(\delta + b_{ii}) \leq 0.$$

Therefore, the prefix mass $\sum_{j \leq m} A_\delta(i, j)$ is monotonically decreasing in δ for every $m < i$, which is precisely the rowwise stochastic dominance

$$\delta \geq 0 \Rightarrow A_\delta(i, \cdot) \succeq A_0(i, \cdot), \quad \delta \leq 0 \Rightarrow A_\delta(i, \cdot) \preceq A_0(i, \cdot),$$

in the FOSD sense used throughout (equivalently, all prefix masses $\sum_{j \leq m}$ for $m < i$ decrease (increase) with δ). Since $R_\delta(i, \cdot) = (1 - \lambda)\delta_i + \lambda A_\delta(i, \cdot)$, the same rowwise dominance holds for the residual kernels:

$$\delta \geq 0 \Rightarrow R_\delta(i, \cdot) \succeq R_0(i, \cdot), \quad \delta \leq 0 \Rightarrow R_\delta(i, \cdot) \preceq R_0(i, \cdot).$$

Now consider the depth- T rollout $P^{(T)} = R^{(T)} \cdots R^{(1)}$ and fix an output index i . Let $\mu_0 = \nu_0 = \delta_i$, and define recursively

$$\mu_t := \mu_{t-1} R_{\delta^{(t)}}^{(t)}, \quad \nu_t := \nu_{t-1} R_0^{(t)},$$

so that μ_T is the i -th row of $P^{(T)}$ and ν_T is the i -th row of the baseline rollout $P^{(T)}|_{\delta^{(1:T)} \equiv 0}$. Assume first that $\delta^{(t)} \geq 0$ for all t . We prove by induction that $\mu_t \succeq \nu_t$ for all t . Indeed, if $\mu_{t-1} \succeq \nu_{t-1}$, then by the rowwise dominance above and Lemma A.4,

$$\mu_{t-1} R_{\delta^{(t)}}^{(t)} \succeq \mu_{t-1} R_0^{(t)},$$

and by stochastic monotonicity of $R_0^{(t)}$ together with Lemma A.2,

$$\mu_{t-1} R_0^{(t)} \succeq \nu_{t-1} R_0^{(t)}.$$

Chaining yields $\mu_t \succeq \nu_t$. Since $\mu_0 = \nu_0$, we conclude $\mu_T \succeq \nu_T$. Unpacking the definition of \succeq gives that for every $k < i$,

$$\sum_{j=1}^k P_{ij}^{(T)} \leq \sum_{j=1}^k P_{ij}^{(T)} \Big|_{\delta^{(1:T)} \equiv 0}.$$

If instead $\delta^{(t)} \leq 0$ for all t , all inequalities reverse and we obtain

$$\sum_{j=1}^k P_{ij}^{(T)} \geq \sum_{j=1}^k P_{ij}^{(T)} \Big|_{\delta^{(1:T)} \equiv 0}, \quad \forall k < i.$$

This is exactly the claimed signed drift: positive diagonal content increases recency (reduces prefix mass), while negative diagonal content increases primacy (increases prefix mass). \square

A.2. Proof of Theorem 5.4 (Infinite-Depth Case)

We recall the residual-aware transition $R^{(t)} = (1 - \lambda_t)I + \lambda_t A^{(t)}$ and the rollout $P^{(T)} = R^{(T)}R^{(T-1)} \dots R^{(1)}$.

Proof of Lemma 5.3. To prove (i), we expand the residual dynamics $X^{(t)} = P^{(t)}X^{(0)}V^{(t)}$, where

$$P^{(t)} := \prod_{s=1}^t R^{(s)}, \quad V^{(t)} := \prod_{s=1}^t W_V^{(s)}.$$

Since each $R^{(s)}$ is row-stochastic, their product $P^{(t)}$ is also row-stochastic. Thus, each row $X_{i,:}^{(t)}$ is a convex combination of the rows of $X^{(0)}V^{(t)}$. By the properties of the operator norm and Assumption 5.2:

$$\|X_{i,:}^{(t)}\|_2 \leq \sum_{k=1}^n P_{ik}^{(t)} \|X_{k,:}^{(0)}V^{(t)}\|_2 \leq \sum_{k=1}^n P_{ik}^{(t)} (CC_V) = CC_V.$$

Setting $C_X = CC_V$ establishes the uniform bound on trajectories.

For (ii), we utilize the result of part (i). The attention logits are given by $s_{ij}^{(t)} = (X_{i,:}^{(t)}W_Q^{(t)})(X_{j,:}^{(t)}W_K^{(t)})^\top$. By Cauchy-Schwarz and Assumption 5.1:

$$|s_{ij}^{(t)}| \leq \|X_{i,:}^{(t)}\|_2 \|W_Q^{(t)}\|_2 \|X_{j,:}^{(t)}\|_2 \|W_K^{(t)}\|_2 \leq (C_X C)^2 =: M.$$

Since M depends only on the sequence length and fixed constants, using the same softmax lower bound as in Wu et al. (2025), ε is a strictly positive universal lower bound. \square

Proof of Theorem 5.4(i). Assume $\sum_{t=1}^\infty \lambda_t < \infty$. We first lower bound the diagonal entries of $R^{(t)}$ using Lemma 5.3:

$$R_{ii}^{(t)} = (1 - \lambda_t) + \lambda_t A_{ii}^{(t)} \geq 1 - \lambda_t + \lambda_t \varepsilon = 1 - (1 - \varepsilon) \lambda_t.$$

Since $P^{(T)}$ is a product of non-negative matrices, the diagonal of the product is at least the product of the diagonals:

$$P_{ii}^{(T)} = (R^{(T)} \dots R^{(1)})_{ii} \geq \prod_{t=1}^T R_{ii}^{(t)} \geq \prod_{t=1}^T (1 - (1 - \varepsilon) \lambda_t).$$

Since $\sum \lambda_t < \infty$, the infinite product $\prod_{t=1}^\infty (1 - (1 - \varepsilon) \lambda_t)$ converges to a strictly positive constant. Thus, $\liminf_{T \rightarrow \infty} P_{ii}^{(T)} > 0$, and the attention mass cannot collapse entirely to the first token. \square

Proof of Theorem 5.4(ii). Assume $\sum_{t=1}^\infty \lambda_t = \infty$. For any token i , we track the total weight $W_{i,>1}^{(T)}$ assigned to all positions excluding the first token. Since each attention matrix $A^{(t)}$ must assign at least ε mass to the first token, it reduces the remaining weight by a factor of at least $(1 - \varepsilon)$.

The residual $R^{(t)} = (1 - \lambda_t)I + \lambda_t A^{(t)}$ acts as a weighted average between maintaining the current weight distribution and applying this reduction. Consequently, the weight assigned to positions $j > 1$ shrinks at each layer by a factor of $(1 - \varepsilon \lambda_t)$. By compounding these contractions through the rollout $P^{(T)}$, we obtain:

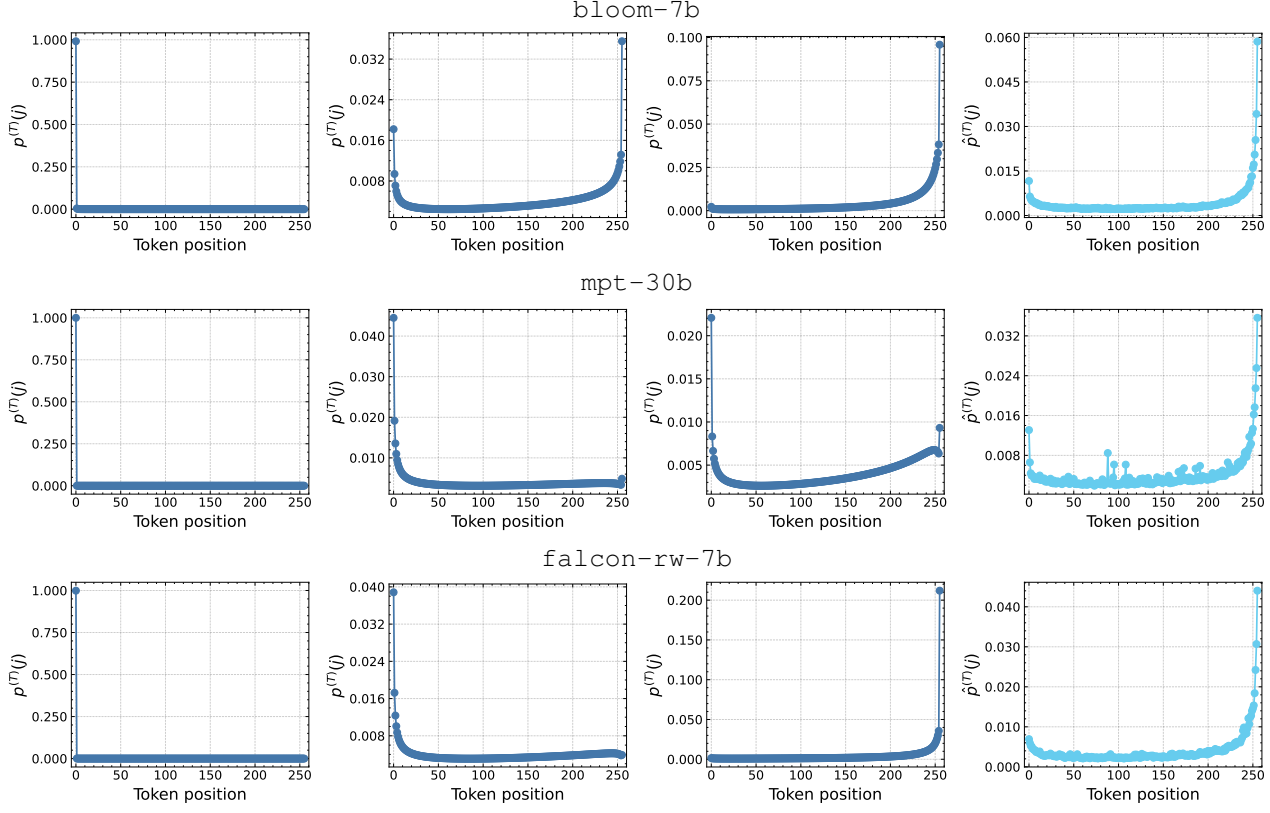
$$R_{jj}^{(t)} = (1 - \lambda_t) + \lambda_t A_{jj}^{(t)} \leq 1 - \lambda_t + \lambda_t (1 - (j-1)\varepsilon) = 1 - (j-1)\varepsilon \lambda_t.$$

For the rollout $P^{(T)} = R^{(T)} \dots R^{(1)}$, since these are lower-triangular matrices, the diagonal entries of the product are the products of the diagonal entries:

$$P_{jj}^{(T)} = \prod_{s=1}^T R_{jj}^{(s)} \leq \prod_{s=1}^T (1 - (j-1)\varepsilon \lambda_s) \leq \exp \left(-(j-1)\varepsilon \sum_{s=1}^T \lambda_s \right).$$

For $j > 1$, the divergence of $\sum \lambda_s$ implies $P_{jj}^{(T)} \rightarrow 0$ as $T \rightarrow \infty$. By induction on the lower-triangular structure, the off-diagonal entries $P_{ij}^{(T)}$ for $j > 1$ also decay at this rate, i.e., $P_{ij}^{(T)} \leq C' \exp(-(j-1)\varepsilon \sum \lambda_s)$.

As $T \rightarrow \infty$, the divergence of $\sum \lambda_t$ forces this upper bound to zero. This implies that the attention mass for all tokens $j > 1$ vanishes, leaving the first token to absorb the entire unit of row mass: $\lim_{T \rightarrow \infty} P_{i1}^{(T)} = 1$. \square



(a) Attention-only rollout (b) Residual-aware rollout. (c) Residual-aware rollout with constant content. (d) Measured input token influence.

Figure 3. Final-token influence distribution $p^{(T)}$ for the 30-layer `bloom-7b` (top row) and the 48-layer `mpt-30b` (middle row) and the 36-layer `falcon-rw-7b` (bottom row), computed using our residual-aware rollout theory (Sections 3 and 4) and compared to the empirically estimated final-token input token influence $\hat{p}^{(T)}$ (Section 6.3). See Section 6 for details.

B. Additional Rollout and Influence Analysis

This appendix provides additional qualitative and quantitative results for the controlled rollout experiments discussed in Section 6. We report final-token rollout distributions $p^{(T)}$ computed using the residual-aware rollout theory defined in Section 3, together with the corresponding empirically measured input token influence distributions $\hat{p}^{(T)}$ (Section 6.3), for a range of ALiBi-based Transformer models.

B.1. Qualitative Comparison of Rollout and Measured Influence

Figure 3 shows additional rollout and measurement curves across models. Across all examined cases, the empirically measured influence distributions exhibit a characteristic U-shaped profile, reflecting an architectural positional prior induced by causal masking and residual connections. The residual-aware rollout without content recovers this U-shaped structure, while incorporating constant-plus-diagonal content modulates the profile by shifting mass toward later positions without eliminating the underlying shape. In contrast, the attention-only rollout collapses to the first token and fails to reproduce the empirical pattern.

B.2. Quantitative Agreement Between Theory and Measurement

To quantify the agreement between the predicted influence distributions $p^{(T)}$ and the empirically measured input token influence $\hat{p}^{(T)}$, we report Spearman rank correlation and normalized 1-Wasserstein distance on token positions, using the ground metric $d(i, j) = |i - j|/(n - 1)$ (Tables 4 and 5). Across datasets, Spearman correlations are consistently high, indicating that the rollout theory accurately captures the ordering of influential positions. This agreement is particularly

Table 4. Spearman rank correlation (\uparrow higher is better) between controlled rollout variants and empirically measured input token influence, reported per dataset. Column a) corresponds to attention-only, column b) to residual-aware, and column c) to residual-aware with constant content rollouts.

Model	FineWeb-Edu			DCLM-Baseline			Wikipedia		
	(a) Attn. only	(b) Res.- aware	(c) Res.-aware + const. content	(a) Attn. only	(b) Res.- aware	(c) Res.-aware + const. content	(a) Attn. only	(b) Res.- aware	(c) Res.-aware + const. content
falcon-rw-7b	-0.52	0.60	0.90	-0.81	0.62	0.88	-0.83	0.61	0.90
mpt-7b	-0.43	0.88	0.53	-0.35	0.79	0.47	-0.56	0.93	0.68
mpt-30b	-0.56	0.62	0.81	-0.47	0.61	0.63	-0.68	0.48	0.83
bloom-7b	-0.44	0.83	0.50	-0.35	0.77	0.41	-0.58	0.93	0.66
bloom-176b	-0.57	0.91	0.83	-0.52	0.86	0.80	-0.49	0.98	0.96

Table 5. Wasserstein distance (\downarrow lower is better) between controlled rollout variants and empirically measured input token influence, reported separately per dataset. Column a) corresponds to attention-only, column b) to residual-aware, and column c) to residual-aware with constant content rollouts.

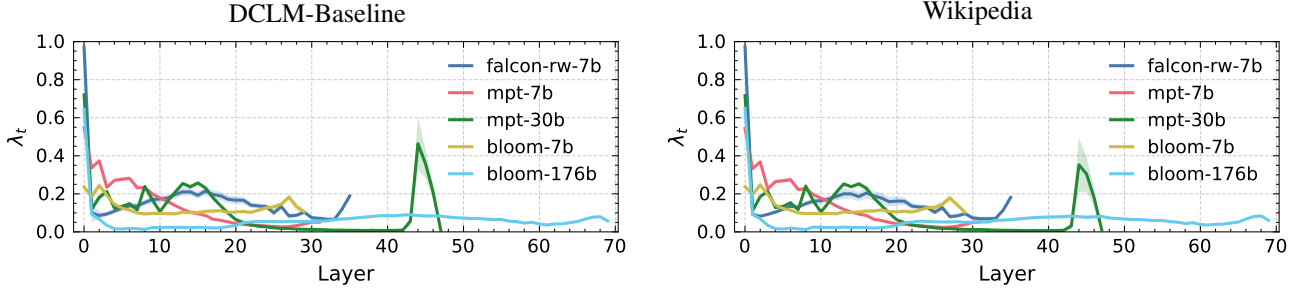
Model	FineWeb-Edu			DCLM-Baseline			Wikipedia		
	(a) Attn. only	(b) Res.- aware	(c) Res.-aware + const. content	(a) Attn. only	(b) Res.- aware	(c) Res.-aware + const. content	(a) Attn. only	(b) Res.- aware	(c) Res.-aware + const. content
falcon-rw-7b	0.63	0.19	0.16	0.66	0.19	0.15	0.68	0.21	0.13
mpt-7b	0.62	0.09	0.10	0.59	0.06	0.12	0.66	0.13	0.06
mpt-30b	0.61	0.16	0.05	0.58	0.14	0.03	0.65	0.20	0.09
bloom-7b	0.63	0.04	0.18	0.61	0.03	0.18	0.67	0.08	0.14
bloom-176b	0.65	0.08	0.01	0.63	0.06	0.02	0.69	0.11	0.05

pronounced for larger models, such as `mpt-30b` and `bloom-176b`, suggesting that the simplifying assumptions underlying the theory become increasingly accurate with depth. At the same time, the Wasserstein distances are uniformly small, demonstrating that the predicted influence distributions are not only rank-consistent but also closely match the empirical distributions in shape.

Taken together, the qualitative and quantitative results show that Transformer architectures induce a strong U-shaped positional prior even in the absence of content, and that incorporating a coarse content abstraction yields predicted influence distributions that closely align with empirical measurements. These findings support the view that the residual-aware rollout theory provides a quantitatively faithful approximation of influence propagation in pretrained Transformer models.

C. Residual Mixing Schedules

We additionally report measurements (Figure 4) of the depth-wise effective residual mixing schedule $\{\lambda_t\}$, defined in Equation (5), on DCLM-Baseline and Wikipedia (Figure 4). These estimates serve as key empirical inputs to our residual-aware rollout analysis (Sections 3 and 6).



(a) Mean \pm 95% confidence interval of λ_t over 1,000 samples of length 2,048 from the DCLM-Baseline dataset.

(b) Mean \pm 95% confidence interval of λ_t over 1,000 samples of length 2,048 from the Wikipedia dataset.

Figure 4. Depth-wise effective residual mixing λ_t coefficient (defined in Equation (5)) for different datasets. λ_t quantifies the fraction of each layer's attention update relative to the sum of residual stream and attention contributions.

D. Content Score Heatmaps and Similarity Statistics

This appendix provides representative heatmaps (Figure 5) used in Section 6 to validate the content-logit model from Proposition 4.5. Specifically, for ALiBi models we visualize the mean pre-softmax content scores (i.e., the attention scores before adding the positional bias term and before applying the softmax), averaged over 1,000 prompts. These averages reveal a characteristic constant off-diagonal structure together with a systematic diagonal shift, consistent with the constant-plus-diagonal model in Proposition 4.5.

Distributional evidence for constant-plus-diagonal structure. Visual inspection of Figure 5 suggests that, after averaging over prompts, content scores are nearly constant within the diagonal and within the (masked) off-diagonal region. To quantify this effect, we compute within-region homogeneity statistics on the mean content-score matrices averaged over all layers and heads for each model. We report model-level averages of these statistics in Table 6.

Table 6. Mean \pm standard deviation of distributional similarity statistics computed from the *mean* pre-softmax content-score matrices at sequence length $n = 256$, aggregated over all layers and heads for each model. Within-diag similarity and Within-off-diagonal Shannon similarities are computed on the diagonal and strictly lower-triangular entries, respectively. High similarity indicates more homogeneous values within a region, consistent with the constant-plus-diagonal structure assumed in the theoretical analysis.

Model	Within-diag similarity	Within-off-diag similarity
falcon-rw-7b	0.53 ± 0.15	0.45 ± 0.16
mpt-7b	0.58 ± 0.16	0.47 ± 0.20
mpt-30b	0.75 ± 0.18	0.73 ± 0.17
bloom-7b	0.54 ± 0.18	0.47 ± 0.20
bloom-176b	0.86 ± 0.13	0.84 ± 0.14

Specifically, we compute the normalized Shannon entropy separately for the sets of diagonal and off-diagonal entries, which we refer to as the *within-diagonal* and *within-off-diagonal* similarity statistics. These statistics measure the degree to which entries within each region concentrate around a single value.

Let $p \in \Delta^{B-1}$ denote the empirical histogram over B bins computed from a given set of entries (diagonal or off-diagonal). We define the normalized Shannon similarity as

$$\text{Sim}_{\text{Sh}}(p) = 1 - \frac{H(p)}{\log B}, \quad H(p) = - \sum_{i=1}^B p_i \log p_i. \quad (9)$$

Thus $\text{Sim}_{\text{Sh}}(p) \in [0, 1]$, with larger values indicating more homogeneous entries within the region.

High within-region similarity for both diagonal and off-diagonal entries supports the approximation of content logits by a constant background plus a diagonal offset, as assumed in Proposition 4.5.

Overall, the within-region similarities are moderate to high across all models, indicating that both diagonal and off-diagonal entries are comparatively homogeneous in the mean content-score matrices. This effect is most pronounced for bloom-176b, where both similarity metrics approach unity, suggesting that the constant-plus-diagonal approximation is particularly accurate for larger models. Taken together, these statistics confirm that (i) diagonal entries cluster around a common level and (ii) off-diagonal entries cluster around another common level, providing quantitative support for the theoretical model assumed in Proposition 4.5.

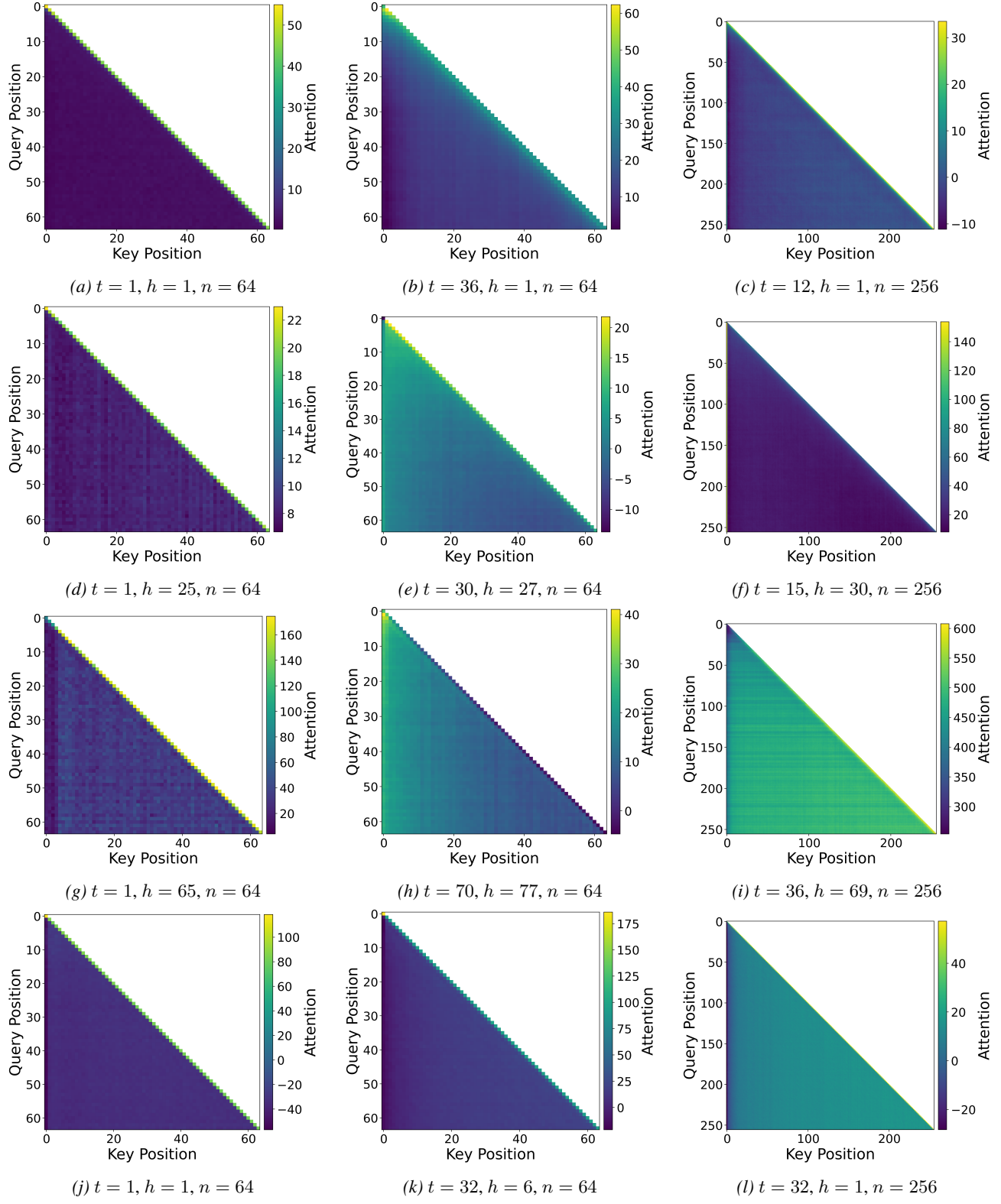


Figure 5. Mean pre-softmax content-score heatmaps for ALiBi-based models. Rows correspond to falcon-rw-7b, bloom-7b, bloom-176b, and mpt-7b (top to bottom). Each panel shows mean pre-softmax content scores averaged over 1,000 FineWeb-Edu prompts for the indicated layer t , head h , and sequence length n (reported in the subcaptions).